1
Synthesis of Polymer Nanocomposites: Review of Various Techniques

Joel Fawaz and Vikas Mittal

1.1
Introduction

Polymer nanocomposites are hybrid organic–inorganic materials with at least one dimension of the filler phase less than 100 nm [1]. Polymer nanocomposites are synthesized via various methods that can be categorized into four major routes: melt intercalation, template synthesis, exfoliation adsorption, and *in situ* polymerization intercalation [1–6]. On the basis of the method and materials used, three types of microstructure can be obtained: unintercalated (or microcomposite), intercalated (and/or flocculated), or exfoliated (or delaminated), as shown in Figure 1.1.

Melt intercalation is the typical standard approach for synthesizing thermoplastic polymer nanocomposites. It involves annealing the polymer matrix at high temperatures, adding the filler, and finally kneading the composite to achieve uniform distribution, as illustrated in Figure 1.2. It has the advantage of being environmental friendly because of the lack of solvent usage. In addition, it is considered compatible with industrial processes such as injection molding and extrusion, which makes it more convenient to utilize and, thus, more economical. However, the high temperatures used in the process can damage the surface modification of the filler. For example, organoclays modified with alkyl ammonium usually decompose at temperatures higher than 140 °C; however, the processing temperature of melt intercalation is in the range of 190–220 °C [4]. Therefore, optimization of the processing conditions is a very important factor that plays a big role in achieving good dispersion and exfoliation. For instance, operating at lower temperatures or using more thermally stable modifications can avoid degradation [1]. Weak electrostatic forces among the filler interlayers and compatibility with the polymer matrix allow the polymer to crawl into the interlayers forming intercalated or exfoliated nanocomposites [6].

Exfoliation adsorption, also called polymer or prepolymer intercalation from solution, is based on a solvent in which the polymer or prepolymer is soluble. The layered silicate, for instance, is first swollen and dispersed in solvent before mixing it with the polymer solution. The polymer chains then intercalate and displace the

Synthesis Techniques for Polymer Nanocomposites, First Edition. Edited by Vikas Mittal.

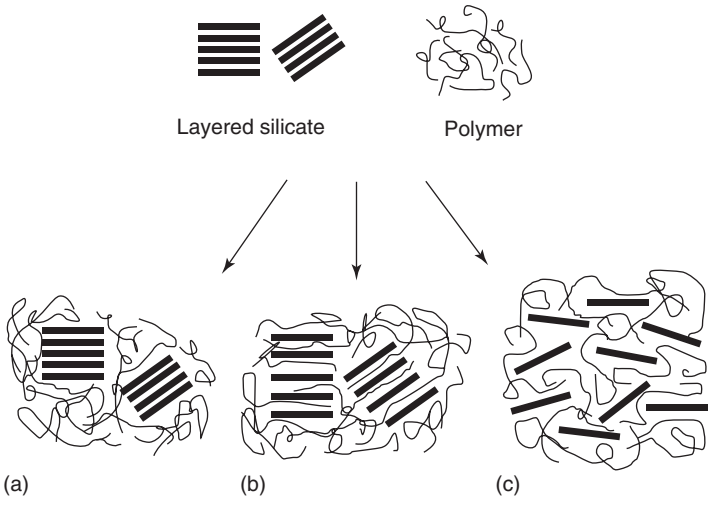

Figure 1.1 Types of composite microstructures: (a) Unintercalated (Phase separated (microcomposite)), (b) intercalated (Intercalated (nanocomposite)), and (c) exfoliated (nanocomposite). Reproduced from [6] with permission from Elsevier.

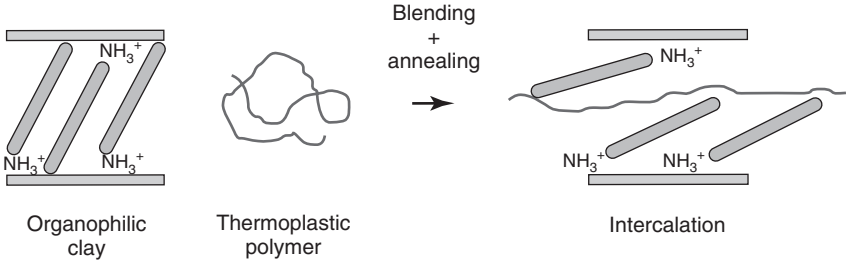

Figure 1.2 The melt intercalation process. Reproduced from [3] with permission from Elsevier.

solvent within the silicate interlayers. Eventually, on removal of the solvent, a multilayer structure is formed as the sheets reassemble trapping the polymer chains, as shown in Figure 1.3 [2, 5, 6]. This approach is widely used for water-soluble polymers to produce intercalated nanocomposites based on polymers with low or no polarity such as poly (vinyl alcohol), poly (ethylene oxide), poly (vinylpyrrolidone), or poly (acrylic acid) [3, 6]. However, unlike melt intercalation, this method is environmentally unfriendly because of the usage of large amounts of solvents. Emulsion polymerization is considered to be under this method as monomers, usually methyl methacrylate and styrene, are dispersed in water along with an emulsifier and different silicate concentrations [5]. The monomer is polymerized with a part of silicate embedded inside the polymer particle and a part adsorbed on the particle surface, forming a nanocomposite.

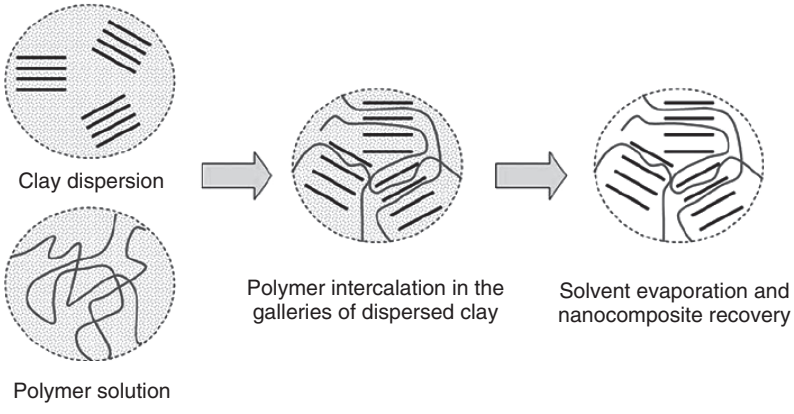

Figure 1.3 The exfoliation adsorption process. Reproduced from [3] with permission from Elsevier.

In situ polymerization involves the swelling of the filler in liquid monomer or monomer solution as the low-molecular-weight monomer seeps in between the interlayers causing the swelling [5]. Polymerization starts either using heat, radiation, initiator diffusion, or by organic initiator or catalyst fixed through cationic exchange [6]. The monomers then polymerize in between the interlayers forming intercalated or exfoliated nanocomposites. The advantage of this approach lies in the better exfoliation achieved compared to melt and exfoliation adsorption methods [4]. Figure 1.4 illustrates the synthesis of nylon-6/clay nanocomposite via *in situ* polymerization in which clay is dispersed in caprolactam monomer and under polymerization conditions, an exfoliated nanocomposite is formed.

Template synthesis, also known as sol-gel technology, is based on an opposite principle than the previous methods. This approach involves the formation of the inorganic filler in an aqueous solution or gel containing the polymer and the filler building blocks [1, 3–6]. The polymer serves as a nucleating agent and promotes the growth of the inorganic filler crystals. As those crystals grow, the polymer is trapped within the layers and thus forms the nanocomposite. It is mainly used for the synthesis of double-layer hydroxide-based nanocomposite and is much

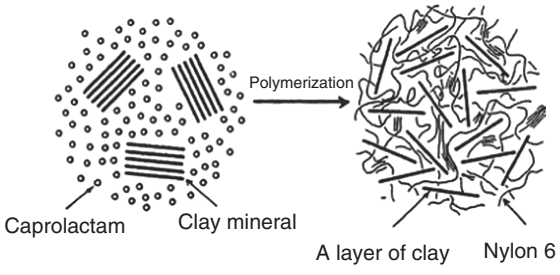

Figure 1.4 Schematic example of *in situ* polymerization process involving the synthesis of nylon-6/clay nanocomposite. Reproduced from [2] with permission from Elsevier.

less developed for the synthesis of layered silicates. This is because of the high temperature used during synthesis that degrades the polymer and the resulting aggregation tendency of the growing inorganic crystals [3, 5]. Therefore, this process is not commonly used.

Till now, only a brief introduction to each method has been provided. However, this chapter focuses on discussing the recent studies conducted in each of the three main respective synthesis methods. Different types of fillers, such as carbon nanotubes (CNTs), silicates, and clay and graphene/graphite oxide, are inclusive in this review. This chapter also analyzes nontraditional methods such as microwave assisted and redox reactions. The readers are referred to these review papers for further reading [1–9].

1.2 Synthesis Methods

1.2.1 Melt Intercalation

As discussed earlier, melt intercalation is considered environmental friendly and a much better substitution for solution mixing, if permittable. However, processing conditions, surface modification of fillers, and compatibility of filler and polymer matrix all play important roles in determining how well the dispersion can be achieved. Alig *et al*. [10] discussed the relation between processing conditions and morphologies obtained for CNT nanocomposites. Moreover, the authors explained the dispersion process by breaking it into four steps: (i) Wetting of initial agglomerates by the polymer, (ii) infiltration of polymer chains into the initial agglomerates to weaken them, (iii) dispersion of agglomerates by rupture and erosion, and (iv) distribution of individualized nanotubes into the matrix. Similarly, Pavlidou and Papaspyrides [3] explained the thermodynamics behind, and the effects of multiple conditions on, melt intercalation for polymer/layered silicates. The entropy loss, associated with the confinement of a polymer melt, is balanced with an entropy gain that is associated with layer separation and greater conformational energy of aliphatic chains of alkylammonium cations. Therefore, it is generally agreed that melt intercalation depends on the surface energies of polymer and modified layered silicates [3].

Junior *et al*. [11] reported the synthesis of recycled high-impact polystyrene (PS)/organoclay nanocomposites by melt intercalation. The processing was done in an interpenetrating corotating twin screw extruder with screw diameter of 20 mm and L/D ratio of 36. Two different speeds and two types of clay fillers (Viscogel S4 and S7 montmorillonite clays), each with different surfactant, were used. Temperature varied between 150 and 190 °C in the processing zones. The high-impact PS was milled before mixing in order to increase the surface area and facilitate dispersion. It was reported that the higher mixing speed of

600 rpm yielded nanocomposites with better dispersion than the ones processed at 450 rpm.

Poly(ε-caprolactone) (PCL)/organo-modified montmorillonites (MMTs) nanocomposites are synthesized in a corotating twin screw extruder whose length is 1200 mm and L/D ratio of 48 [12]. The extrusion was conducted at 140 °C at 250 rpm and 3 kg h^{-1} polymer flow. However, masterbatches of different types of organoclay were prepared to be fed into the extruder rather than following direct addition. Mixed intercalated or exfoliated structures were obtained with different clay material as the nanocomposite prepared with C30B® clay mineral yields an intercalated/exfoliated structure whereas Nanofils5® and Nanofils2® give rise to intercalated nanocomposite Figure 1.5 shows the transmission electron microscope (TEM) images used to characterize the nanocomposites at 3 wt% loading. However, rheological tests showed that better dispersion was obtained for the nonpolar Nanofils2® and this was reflected in the enhancement of the respective thermal and mechanical properties.

Maiti *et al*. [13] reported the preparation of PCL–multiwalled carbon nanotubes (MWCNTs) mixture via melt blending followed by the synthesis of polycarbonate/ε-PCL–MWCNT nanocomposite. A masterbatch of PCL–MWCNT with 3.5 wt% MWCNT loading was first prepared via melt blending using internal mixer at 65 °C and 60 rpm for 10 min. Then, the masterbatch was melt mixed with pure PC at 280 °C and 60 rpm for 10 min. This procedure

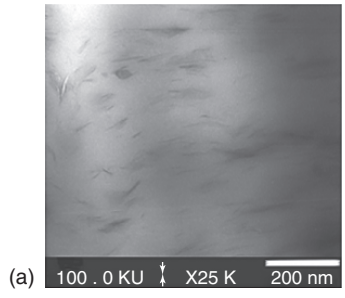

Figure 1.5 TEM images of PCL nancomposites at 3 wt% of: (a) Nanofil5®, (b) C30B®, and (c) Nanofil2®. Reproduced from [12] with permission from Elsevier.

yielded a homogeneous dispersion of CNTs at low loadings as analyzed in scanning electron microscope (SEM). Moreover, through this method, chemical modification of CNTs was not needed as the percolation threshold obtained was at 0.14 wt%. This suggested that an interconnected network was successfully achieved at a low CNT loading.

Other studies conducted by Annala *et al*. [14] and Wang *et al*. [15] utilized the masterbatch process to improve the properties of the final nanocomposites. Annala *et al*. [14] reported the synthesis of poly(methyl methacrylate) (PMMA)/MWCNT and PS/MWCNT using *in situ* polymerized masterbatches that were to be used in corotating twin screw mini-extruder with the capacity of 16 cm^3 and screw length of 150 mm. Different mixing speed and time were investigated to determine the optimum conditions for better properties. Similarly, Wang *et al*. [15] synthesized phthalocyanine (Pc)/MWCNT nanocomposites by placing the prepared masterbatch in a preheated mold at 250 °C and cured at controlled elevated temperatures for 4 h. In both situations, good dispersion of the CNTs was achieved. However, it was noted that depending on the properties of the system, the feeding method of CNTs can affect the properties of the final composite [14].

Tan *et al*. [16] reported a novel approach of synthesizing rubber/clay nanocomposites via latex compounding and melt mixing. In this approach, well-exfoliated masterbatches and intercalated/exfoliated nanocomposites were achieved by using Ca-MMT modified with bis[3-triethoxysilylpropyl-]tetrasulfide (TESPT). This modification enhanced the interface by reacting with the surface groups of Ca-MMT. The masterbatch was first prepared by latex compounding in which the cooled organic clay aqueous suspension was mixed with natural rubber (NR) latex. The mixture was vigorously stirred, co-coagulated in 10% calcium chloride and eventually washed and dried. The masterbatchs were added to a 6-inch two-roll mill along with styrene butadiene rubber (SBR) and epoxidized natural rubber (ENR) to be melt mixed to achieve the nanocomposite. Figure 1.6 shows the X-ray diffraction (XRD) patterns for the pristine Ca-MMT, the masterbatch, and the nanocomposite. It can be noted that an exfoliated structure was obtained in the masterbatch following the absence of peaks. Moreover, this led to an exfoliated/intercalated structure as some of the initial clay in the masterbatch was intercalated by the rubber chains.

A novel approach of melt spinning layered double hydroxide (LDH)/high-density polyethylene (HDPE) nanocomposites prepared by melt extrusion was reported by Kutlu *et al*. [17]. LDHs were hydrophobically modified by carboxylic acid salts of different alkyl chain lengths to improve the lack of compatibility between LDH and polymer matrix. Those modified LDHs were first mixed with PE-g-maleic anhydride (MA) to improve the miscibility of LDH and PE followed by the dilution of masterbatches with HDPE. Then, they were processed in a microcompounder at 190 °C, 100 rpm and 5–10 min mixing time. Different modifiers yielded different interlayer arrangements. Polymer chains were stated to diffuse into LDH galleries because of the high-shearing force, and partial exfoliation was achieved, as supported by XRD and TEM analysis. Myristic acid

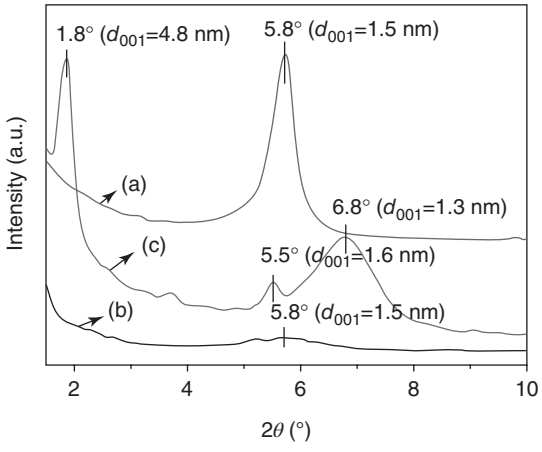

Figure 1.6 XRD patterns for: (a) pristine Ca-MMT, (b) NR/modified Ca-MMT masterbatch, and (c) rubber/clay nanocomposite. Reproduced from [16] with permission from Elsevier.

modified LDH/HDPE nanocomposite showed the highest exfoliation degree at 1 wt% filler level as well as the best processing conditions and mechanical properties of the fiber elements. On the other hand, Mezghani *et al*. [18] reported the synthesis of linear low density polyethylene (LLDPE)/MWCNT nanocomposite fibers prepared via melt extrusion and spun through a spinneret die. The effects of CNT loadings on the properties of LLDPE/MWCNT nanocomposite were investigated and it was noted that on slight addition of CNT, the properties are generally enhanced.

Shanks and Cerezo [19] reported the synthesis of poly(propylene-g-maleic anhydride) (PPMA)/expanded graphite oxide (EGO) nanocomposites. This was done in HAAKE heated kneading mixer for 30 min at 200 °C and 60 rpm. Because of the unpolar nature of PP (polypropylene), a compatibilizer containing polar groups such as MA was required to improve compatibility between the two systems. There was no change in the d-spacing of graphite layers in PPMA/EGO nanocomposites at different EGO loadings, as reported by XRD results. The graphite layers were said to be ordered and multilayered in the final composite.

Unnikrishnan *et al*. [20] reported the synthesis of PMMA/organoclay nanocomposites using a 69-cm^3 batch mixer with roller rotors. Before blending, the different organoclays (C30B®, C10A®, and C93A®) and PMMA pellets were dried for 12 h for better processing. Temperature was set to 180 °C at a rotor speed of 50 rpm for 30 min. It was noted that with the addition of maleic anhydride, as a grafting agent, better intercalation was achieved as investigated in the TEM images. The grafting agent improved the interfacial region between the PMMA and the clay minerals, which led to the intercalation of the polymer chains in between the clay layers. PMMA/C30B® nanocomposite was reported to have an optimum, as well as the highest, d-spacing of 4.16 nm.

Thermoplastic Polyurethane (TPU)/C15A® clay nanocomposites were reported to be synthesized by Barick and Tripathy [21] in HAAKE extruder at 185 °C and

100 rpm rotor speed for 6 min. It was detected by XRD that exfoliated structures were obtained at low loadings of clay minerals because of either high disorder state or the exfoliation of the silicate layers. However, the peak position at $d_{001} = 16.5$ Å and $d_{002} = 36.64$ Å of the clay is shifted to 19.5 and 40.5 Å in 9 wt% loaded nanocomposite, respectively. This indicated the intercalation was achieved above 5 wt% loading. Because of the absence of functional groups on C15A® and high shear stresses from melt processing, mixed exfoliation/intercalation nanocomposites were obtained. Moreover, it was visible and supported in TEM that with increasing clay loading, small clusters of clay particles were observed giving rise to intercalated structures.

Poly(ethylene oxide) (PEO)/clay nanocomposites were reported using Li-MMT [22] and Na-MMT [23]. Erceg *et al*. [22] reported the synthesis of different concentration of PEO/Li-MMT via melt intercalation at 90 °C for 8 h in vacuum oven. The maximum value of interlayer distance of Li-MMT was reported, according to SAXS, to be 1.88 nm (18.8 Å) for 70/30 PEO/Li-MMT nanocomposite. This increase amounts to 56.7% of Li-MMT original value, indicating an intercalated structure. On the other hand, Na^+-modified MMT was used in the synthesis of PEO/clay nanocomposites, as reported by [23]. XRD results showed that the gallery size remained the same (8.3 Å) at different PEO loadings when prepared via melt intercalation unlike when prepared via solution intercalation, as shown in Figure 1.7. This was explained to be because of the stretching of PEO chains as they enter the silicate gallery at low PEO loading in solution intercalation. However, at higher loading, PEO chains reduce their length to accommodate more PEO chains, thus expanding the gallery to 8.3 Å for concentrations higher than 15%. In melt intercalation, the PEO chains diffuse into the silicate gallery

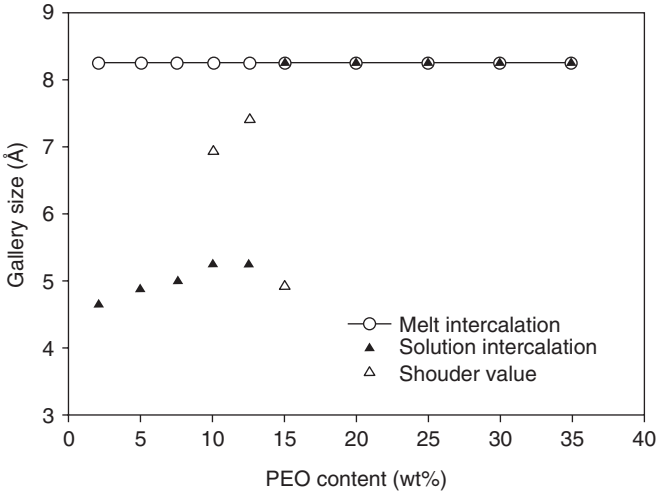

Figure 1.7 Gallery size of PEO/MMT nanocomposites prepared from melt and solution intercalation at different PEO loadings. Reproduced from [23] with permission from Elsevier.

while maintaining their helical structure, achieving the final gallery spacing from the start.

1.2.2 Exfoliation Adsorption

Solution intercalation method can be generally divided into several substeps [24]: (i) dispersion of nanotubes in a solvent by agitation, (ii) mixing of nanotubes and polymer solutions by agitation, and (iii) controlled evaporation of solvent and/or precipitation of nanocomposite. Unlike in melt intercalation, the driving force behind exfoliation adsorption is the entropy gained by the desorption of solvent [2, 3]. This compensates the decreased entropy of the confined intercalated chains. This method is considered good for the intercalation of polymers with little or no polarity [2].

1.2.2.1 Solution Intercalation

Elastomer/graphene nanocomposites were prepared by solution intercalation, as demonstrated in Figure 1.8 [25]. Graphene platelets (~3 nm in thickness)

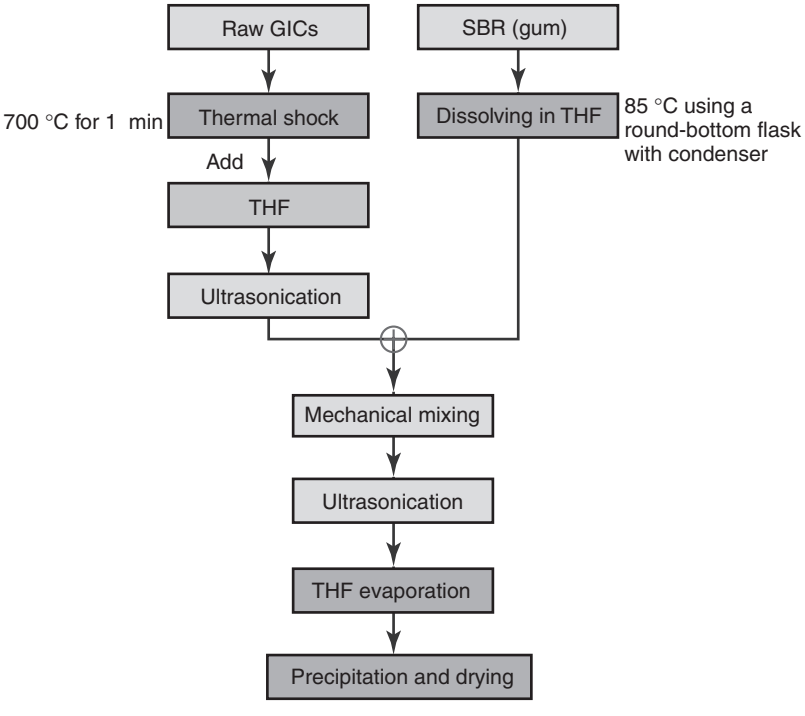

Figure 1.8 Synthesis flowchart for SBR/graphene nanocomposite by solution mixing. Reproduced from [25] with permission from Elsevier.

were obtained from graphite-intercalated compound (GIC) by exposing them to thermal shock and treating them in tetrahydrofuran (THF) solvent while being ultrasonicated. The suspension was then added to the SBR mixture and mechanically mixed at 200 rpm followed by sonication for 1 h below 30 °C. Evaporation of the solvent was done till 60 °C by mechanical stirring in which 60% was evaporated and at 60 °C, ethanol was used to precipitate, collect, wash, and dry the nanocomposite powder. According to XRD and TEM, intercalated structures were obtained. Moreover, the authors compared those results with those obtained from melt mixing, and better exfoliation and dispersion was achieved in the former. This is because more interlayer spacing is available for polymer to intercalate. This was validated with the lower percolation threshold and higher mechanical properties obtained.

Bian *et al*. [26] reported the synthesis of poly(propylene carbonate) (PPC)/modified graphite oxide (MGO) nanocomposites via solution intercalation. MGO was first dispersed in 25 ml dimethylformamide (DMF) for 30 min and then mechanically stirred for 10 min. PPC was then added to the dispersion and stirred for 24 h at 40 °C. Evaporation of the solvent was done in a Petri dish under vacuum at room temperature. The modification of GO (graphite oxide) was necessary considering the incompatibility of hydrophobic PPC with the hydrophilic GO. Therefore, hydroxyl groups were grafted on the GO surface in order to enhance the interfacial adhesion and promote nanocomposite formation. According to XRD results, a d-spacing of 1.7 nm was achieved in PPC/MGO nanocomposites, which is 1.4 nm greater than that in natural graphite powder (= 0.335 nm). This indicated that intercalated/exfoliated structures were obtained. Moreover, enhanced thermal and mechanical properties were obtained as a result of good dispersion of MGO in PPC matrix.

PS/modified laponite clay nanocomposites were synthesized as reported by [27]. Modification of laponite was performed by an ion-exchange reaction with the cationic surfactant cetyltrimethyl ammonium bromide (CTAB). This was done to enhance the compatibility between the clay mineral and the hydrophobic polymer matrix. Good compatibility was achieved as PS chains intercalate into the interlayer spacings of laponite as observed by SEM. However, with increasing laponite, clay loading, aggregation, and agglomeration were observed in the nanocomposite.

Gu *et al*. [28] reported the synthesis of elastomer/organo-MMT nanocomposite via solution intercalation. First, the organo-modified MMT was dispersed in a solvent oil before adding it to the *cis*-1,4-polybutadiene rubber (BR) solution. The mixture was stirred for 30 min at 60 °C and then the solvent was evaporated. The nanocomposite powder was then compounded and cured for specimen preparation. Intercalated structures were obtained as determined by XRD and TEM results in which d-spacing increased from 1.55 nm, for the original MMT, to 3.63 nm in the BR/organo-MMT nanocomposite.

Polyamide (PA)/MWCNTs nanocomposites synthesized via solution mixing are reported in the literature [24, 29]. Functionalized CNTs better disperse the filler in the polymer matrix, as compared to pristine CNTs [29]. Moreover, the use of

initiators to create polymer grafted nanotubes would also help in dispersion [24]. This is because of the enhanced interfacial interaction between the polymer matrix and CNTs. In both cases, good dispersion of CNTs was achieved throughout the polymer matrix.

Another use of MWCNTs as filler materials was reported by Marroquin *et al*. [30]. The authors reported the synthesis of a novel material based on chitosan. Fe_3O_4/MWCNT/chitosan nanocomposites were prepared by solution mixing according to the schematic in Figure 1.9. Fe_3O_4 and MWCNT were ultrasonicated for 1 h in distilled water before adding chitosan and acetic acid. The mixture was magnetically stirred for 2 h followed by ultrasonication for 30 min. The mixture was degassed and vacuum dried to obtain the nanocomposite films. Intercalation with good dispersion was achieved as noted from XRD results following the disappearance of the peak in the MWCNT signal at $2\theta = 26°$ from nanocomposite signals. Fe_3O_4 acted as an antiplasticizer agent that led to higher crystallinity and thus better electrical and mechanical properties.

Zeng *et al*. [31] and Chen *et al*. [32] reported the synthesis of PMMA/MWCNT nanocomposite foams via solution mixing. Solvent casting and antisolvent precipitation methods were used by Zeng *et al*. [31] to prepare the foams in order to investigate the methodology impact on foam morphology and properties. The former involves evaporating the solvent whereas the latter utilizes another solvent to precipitate the nanocomposite from the main solvent. In both cases, uniform dispersion of MWCNTs increased the bubble density and reduced cell size. However, much notable results were reported for the modified antisolvent precipitation method that involves suspending CNTs in a solvent before adding to the polymer solution [31, 32].

In addition to foams, Shirazi *et al*. [33] used solution casting and solvent evaporation methods to synthesize polyvinyl alcohol (PVA)/MWCNT nanocomposite membranes. On the other hand, Chen *et al*. [34] used the coprecipitation process to graft poly(3,4-ethylenedioxythiophene) hollow spheres (b-PEDOT) on MWCNTs and to wrap MnO_2 nanograins on the b-PEDOT. MnO_2/b-PEDOT/MWCNTs hybrid nanocomposite was synthesized as a result and was used to prepare a microsupercapacitor device.

1.2.2.2 **Emulsion Polymerization**

PS/carbon black (CB) nanocomposites were prepared by emulsion polymerization [35]. Synthesis was carried out by first manually mixing CB with styrene monomer at room temperature. A viscous paste was formed as carbon absorbed the monomer. A surfactant was added to reduce the viscosity of the system. This was followed by the addition of Azobisisobutyronitrile (AIBN) initiator to prepare emulsified monomer droplets. In order to disperse the system, a surfactant solution was added in the presence of ultrasound. Eventually, the dispersion was sent to the reactor for polymerization to take place. The conditions were set to be 60 °C, 350 rpm mixing speed, and 120 min reaction time. According to TEM results, as shown in Figure 1.10, two main results were obtained: particle diameter close to 50 nm and high polydispersity and a layer of CB surrounding the polymer

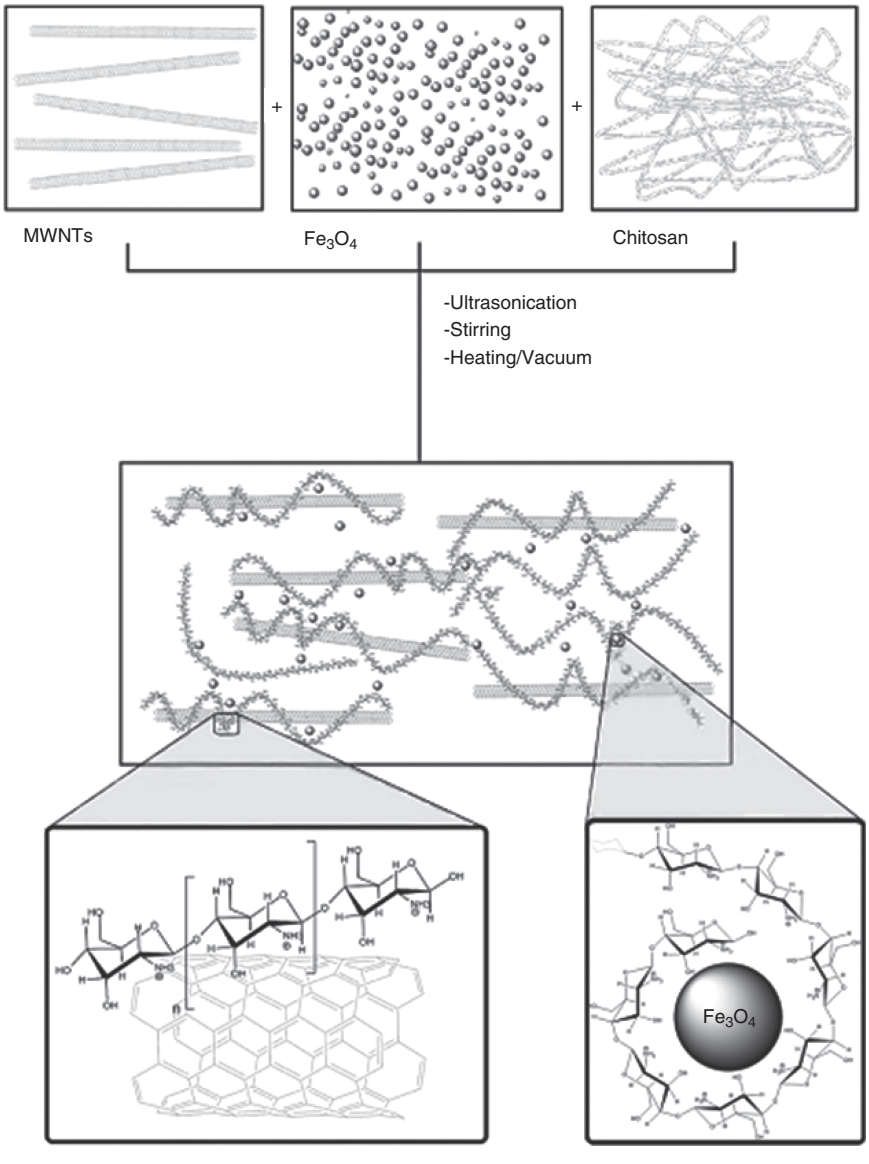

Figure 1.9 Schematic of Fe_3O_4/MWCNT/chitosan nanocomposite synthesis by solution mixing. Reproduced from [30] with permission from Elsevier.

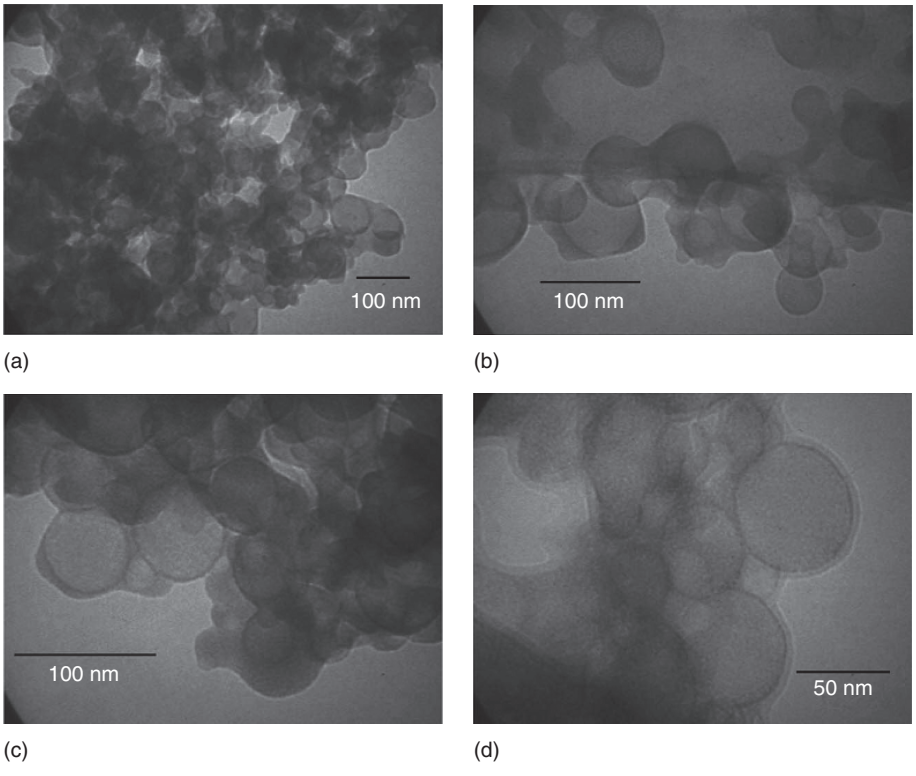

Figure 1.10 TEM images of PS/CB nanocomposite at: (a) 15 k×, (b) 27.5 k×, (c) 38 k×, and (d) 50 k×. Reproduced from [35] with permission from Elsevier.

particles, which is because of carbon primary aggregates being modified during the dispersion stage.

Hassan *et al*. [36] and Hu *et al*. [37] reported the synthesis of PS/graphene nanocomposites. Using sodium dodecyl sulfate (SDS) as a surfactant and stabilizing agent, and ultrasonication, graphene sheets can be obtained from the expanded graphite (EG) that are in turn prepared from the thermal shock of GIC [36]. Graphene nanosheets also can be obtained using hydrazine hydrate in the reaction mixture to reduce GO sheets into graphene [37]. Graphene dispersion was then mixed with styrene monomer, potassium persulfate (KPS) initiator, sodium bicarbonate ($NaHCO_3$) buffer, water, and SDS in a reactor [36]. Conditions were set to 70 °C, 350 rpm, and 3 h reaction time [36]. Figure 1.11 illustrates the synthesis procedure in [37]. Good dispersion and exfoliation was achieved in the final nanocomposite.

Another graphene nanocomposite was prepared by Kuila *et al*. [38] using PMMA as the polymer matrix. The polymerization procedure is similar to that reported by Hu *et al*. GO solution was ultrasonicated before adding SDS aqueous solution. AIBN and styrene monomer were added to the stirred dispersion. Hydrazine monohydrate was added to the mixture that underwent reflux for

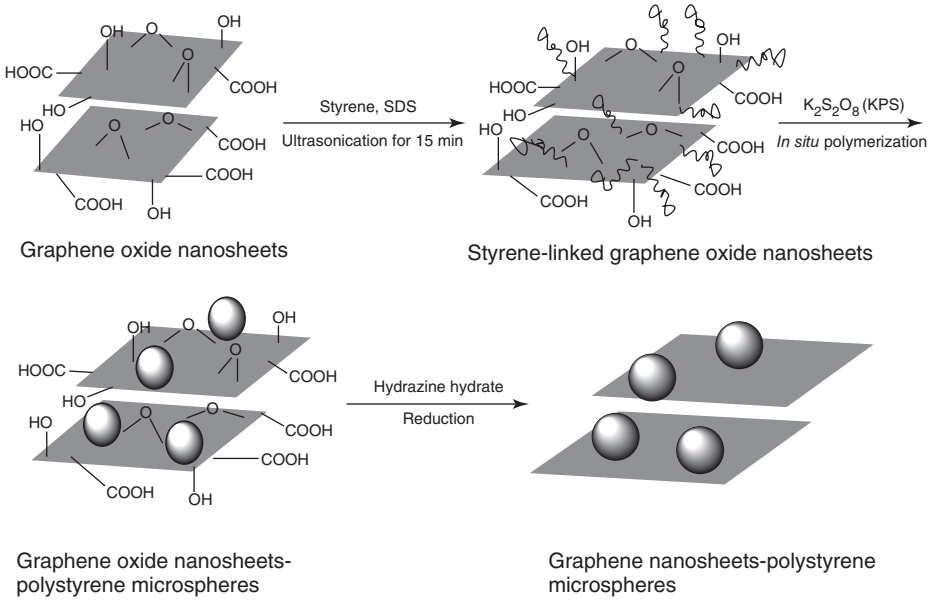

Figure 1.11 Schematic of PS/graphene nanocomposite synthesis. Reproduced from [37] with permission from Elsevier.

additional 16 h to reduce GO to graphene sheets. Eventually, the mixture was precipitated with dilute hydrochloric acid (HCL) and vacuum dried to obtain the nanocomposite. When characterized by XRD, the nanocomposite signals did not show the GO peak. This indicated that GO was successfully reduced to graphene sheets and that their periodic structure was destroyed. According to TEM, the graphene layers were distributed uniformly forming a continuous network.

Polyaniline (PANI)/activated carbon (AC) nanocomposites were synthesized by Oh and Kim [39] using dodecyl benzenesulfonic acid (DBSA). DBSA was used as surfactant and dopant that participated positively in the synthesis of PANI/AC nanocomposites. AC and DBSA aqueous solution were sonicated before adding the aniline monomers followed by intiator. Once the polymerization completed, ethanol was added to precipitate the nanocomposite. The nanocomposite structure can be represented by the schematic in Figure 1.12. It was noted from SEM that with increasing DBSA concentration, the roughness of DBSA-PANI films that cover the surface of AC increases.

Similar to CNTs, inorganic halloysite nanotubes (HNTs) were used as fillers to HIPS nanocomposites [40]. HNTs were uniformly dispersed in the matrix because of PS nanospheres formation on the surface of HNTs, as shown in Figure 1.13. This was prepared by first dispersing the dried HNTs in aqueous SDS. Ammonium persulfate and styrene monomers were added to the stirred solution. Polymerization was done under argon blanket at 70–75 °C and 400 rpm for 18 h. HNTs were also used as filler in epoxy matrix reported by Ye *et al*. [41]. However, in this case, HNTs were not uniformly dispersed in the hybrid material that contained

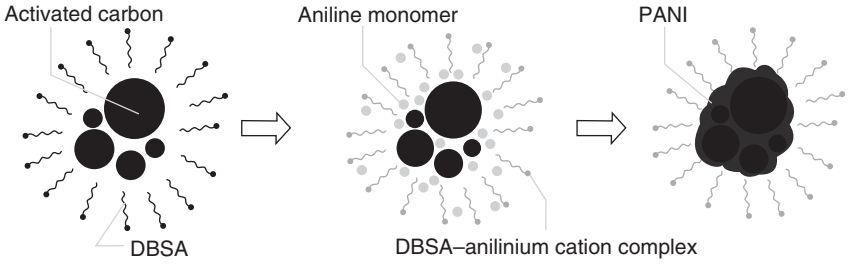

Figure 1.12 Schematic of PANI/AC nanocomposite synthesis. Reproduced from [39] with permission from Elsevier.

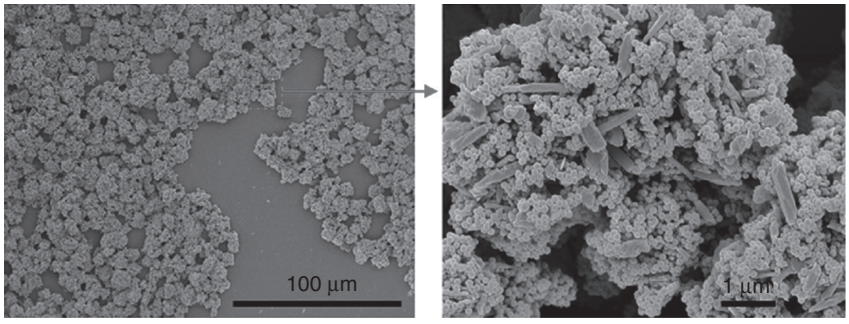

Figure 1.13 (a,b) SEM images of HIPS/HNT nanocomposites. Reproduced from [40] with permission from Elsevier.

carbon fibers. Instead, HNT-rich regions were obtained and were considered as rigid composite particles with high HNT content. This was determined from SEM images, as shown in Figure 1.14. The hybrid material was prepared by dispersing HNTs in acetone while mechanically stirred. Epoxy resin, followed by a curing agent, was added to the degassed mixture. The laminates were then placed in aluminium mold to be cured in a hot pressing agent. They were precured at 80 °C for 2 h and postcured at 160 °C for another 4 h.

Ultrasound can be used to synthesize nanocomposites in emulsion polymerization. Examples are reported by Cetintas and Uyanık [42] and Bhanvase *et al*. [43]. For instance, to synthesize PS/clay nanocomposites, potassium hydroxide and SDS were dissolved in water in three neck round-bottom flask [42]. Meanwhile, styrene monomer and clay minerals were stirred in an ultrasound bath at 0 °C. The two solutions were then mixed together and potassium peroxodisulfate initiator was added. Eventually, the temperature was raised to 50 °C to start the polymerization reaction that lasted 24 h. Finally, the nanocomposite was obtained by precipitation, washing, and vacuum drying. Exfoliated nanocomposites were prepared as determined by XRD results. This was supported by Bhanvase *et al*.

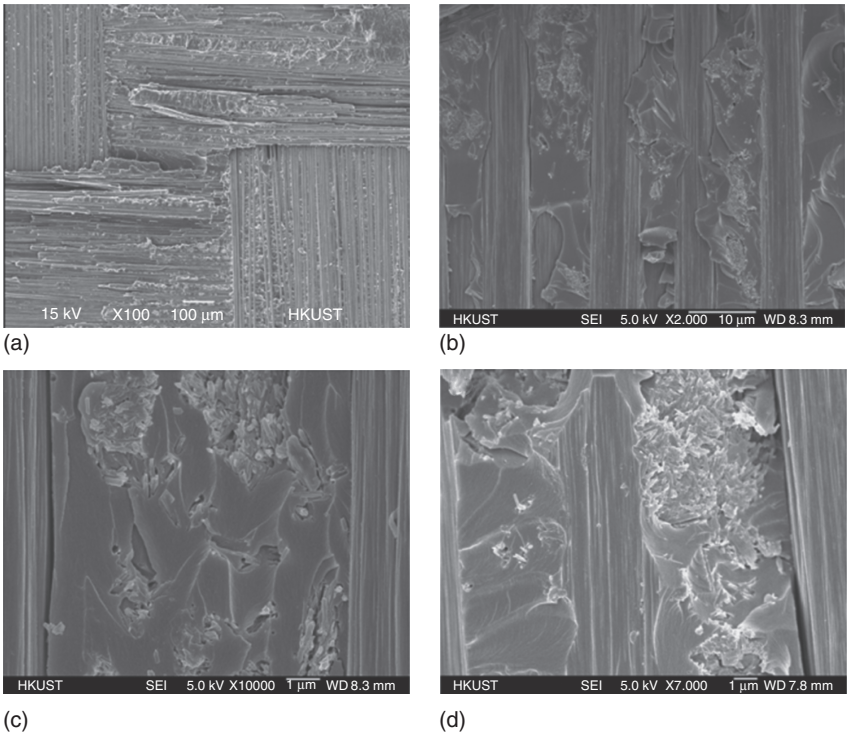

Figure 1.14 (a–d) SEM images of epoxy/HNT/carbon fiber hybrid nanocomposites. Reproduced from [41] with permission from Elsevier.

[43] as their poly(methyl methacrylate-co styrene)/montmorillonite [P(MMA-*co*-St)/O-MMT] nanocomposite was found to be exfoliated with the use of ultrasound. This was determined by XRD as no peaks appeared in the nanocomposite, as shown in Figure 1.15.

1.2.3 *In Situ* Polymerization

Several advantages are attributed to *in situ* polymerization. First of all, thermoplastic- and thermoset-based nanocomposites can be synthesized via this route [3]. In addition, it permits the grafting of polymers on filler surface, which can generally improve properties of the final composite. Partially exfoliated structures can be attainable with this method because of the good dispersion and intercalation of fillers in the polymer matrix. Abedi and Abdouss [4] state that *in situ* polymerization is the most suitable preparation method for polyolefin/clay nanocomposites because of its lack of rigorous thermodynamic requirement compared to the other methods.

Guo *et al*. [44] reported the synthesis of graphene, GO, and functionalized GO – Epoxy nanocomposites via *in situ* polymerization. The synthesis was

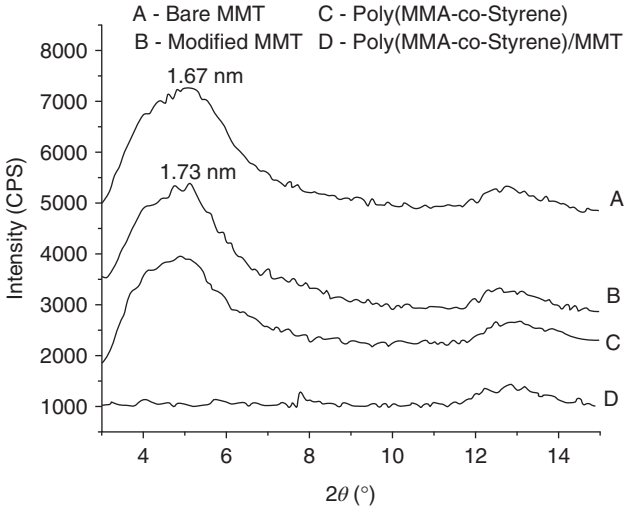

Figure 1.15 XRD signals for: (A) pristine clay, (B) O-MMT, (C) poly(MMA-co-St) polymer, and (D) poly(MMA-co-St)/O-MMT nanocomposite with 4% O-MMT loading. Reproduced from [43] with permission from Elsevier.

carried out by first dispersing the filler in acetone by ultrasonication. The dispersion was then added to the epoxy matrix before placing it in a vacuum oven at 50 °C. *m*-Phenylenediamine was added when 80% of the solvent evaporated, accompanied by vigorous stirring. Eventually, the mixture was poured into a stainless steel mold, dried at 60 °C for 5 h to remove the residual solvent, precured in an oven at 80 °C for 2 h, and postcured at 120 °C for two additional hours to obtain the composites. TEM images, in Figure 1.16, show that better dispersion was achieved in epoxy/graphene and epoxy/functionalized GO nanocomposites compared to epoxy/GO composites. Bundles of GO were visible following Van der Waals and hydrogen bond interactions between GO sheets. On the other hand, absence of polar groups and better interfacial interactions were the reasons behind better dispersion and hair-like structure for other composites.

However, Huang *et al*. [45] reported good dispersion of GO in PP matrix as evaluated in TEM and SEM. In order to do so, Zeigler-Natta (ZN) catalyst was incorporated into GO sheets in the process shown in Figure 1.17. Grignard reagent (RMgCl) was used prior to adding titanium tetrachloride to synthesize GO-supported ZN catalyst. This catalyst was then added at 60 °C to hexane–propylene liquid mixture that is subjected to vigorous stirring. Triethyl aluminium ($AlEt_3$) and dimethoxydiphenylsilane (DDS) initiators were added to the mixture to initiate the polymerization reaction. The final composite was obtained by filtering, washing, and drying.

Other reports of GO composites include PMMA/GO [46] and polypyrrole (PPy)/GO [47]. Exfoliated structures were obtained for both nanocomposites, as suggested by XRD studies. However, according to TEM, agglomeration of GO sheets in PMMA/GO nanocomposite was visible at higher loadings above

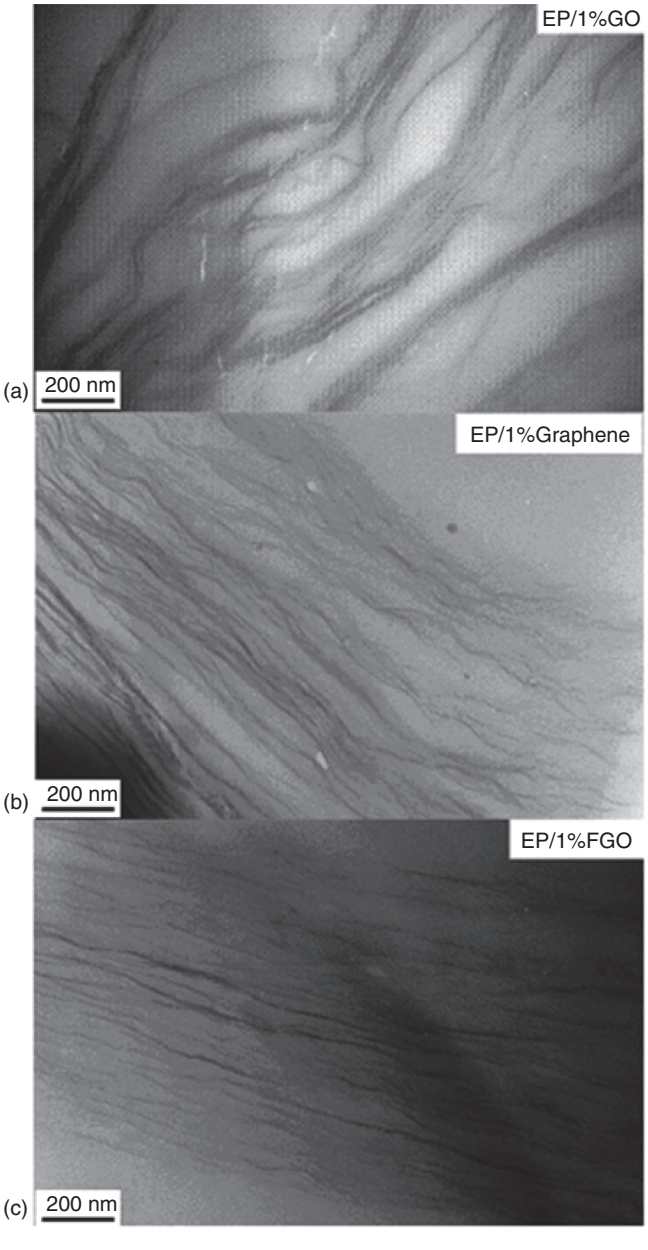

Figure 1.16 (a–c) TEM images of epoxy/graphite nanocomposites. Reproduced from [44] with permission from American Chemical Society.

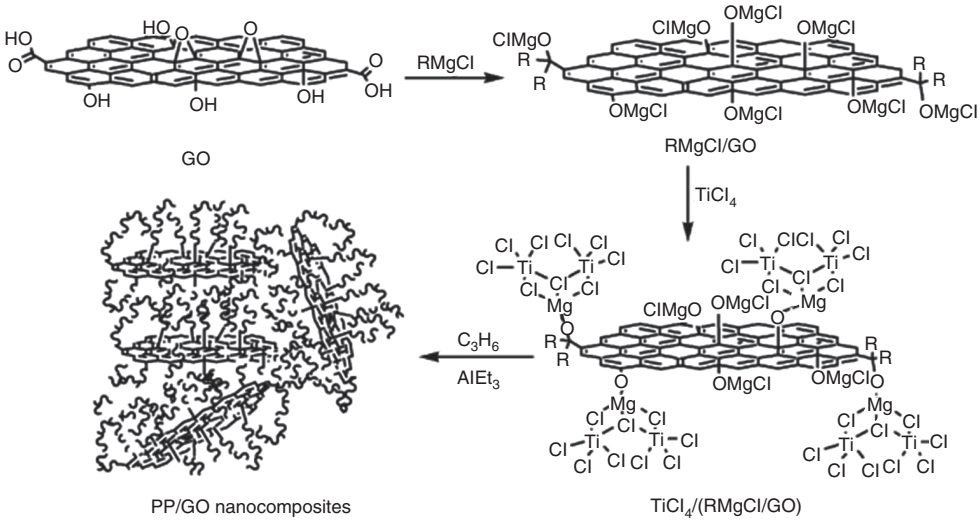

Figure 1.17 Schematic of PP/GO nanocomposite synthesis. Reproduced from [45] with permission from American Chemical Society.

1 wt% [46]. PPy/GO composites were synthesized via liquid–liquid interfacial polymerization, as shown in Figure 1.18. The reason behind the authors using this method instead of the conventional *in situ* polymerization method was its slower and controllable attributes. Moreover, bulk quantities can be prepared by this method.

Intercalated and exfoliated PE/graphite nanocomposites were reported by Fim *et al*. [48]. GIC was first exposed to thermal shock to obtain the EG. In turn, the suspension of EG/ethanol was treated in an ultrasound bath to attain graphite nanosheets (GNSs). Methylaluminoxane (MAO) was used to treat GNS surfaces and as a cocatalyst along with bis(cyclopentadienyl)zirconium dichloride (Cp_2ZrCl_2). The polymerization conditions were as follows: 70 °C, toluene as solvent, 2.8 bar ethylene pressure, and 30 min. Table 1.1 summarizes the XRD data for the nanocomposites. It is noted that with thermal and ultrasound treatment, graphite sheets exfoliated, increasing their interlayer spacing. Moreover, crystal size decreased following agitation and dispersion of graphite, eventually reducing the number of stacked graphene sheets. The 5.6 wt% graphite loading nanocomposite yielded good dispersion with higher interlayer spacing and smaller crystal size. This is because of the polymer chains growing in between the GNSs.

Graphene was used in preparing many nanocomposites via *in situ* polymerization such as nylon-6 (PA-6) [49] and poly(butylene terephthalate) (PBT) [50] – graphene composites. Moreover, ring opening polymerization was used to prepare those nanocomposites. In both cases, good dispersion of graphene was achieved because of the enhanced interfacial interactions [49, 50]. Table 1.2 summarizes XRD results for PBT/graphene nanocomposites. It is noted that at

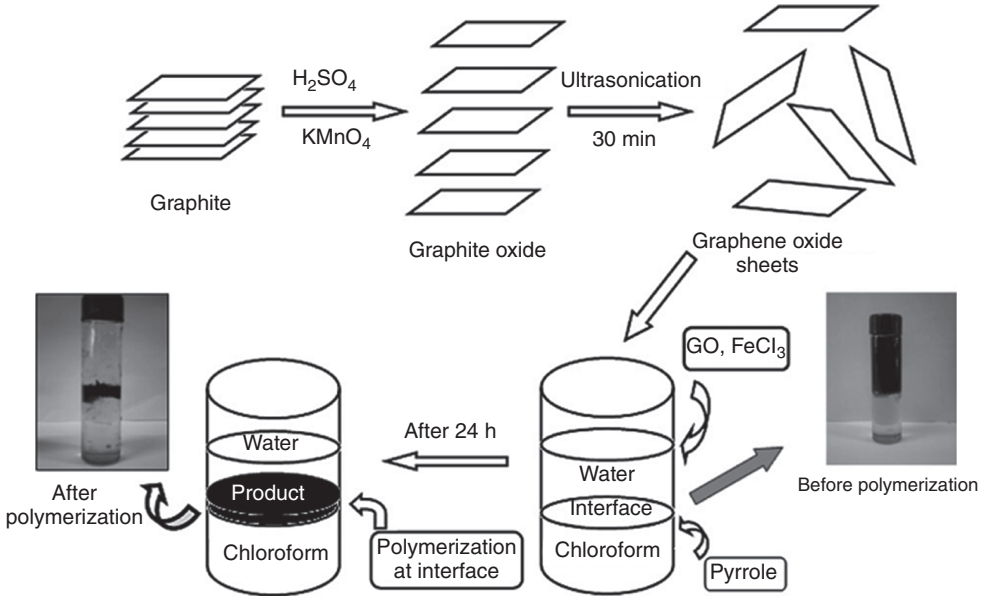

Figure 1.18 Schematic of liquid-liquid interfacial polymerization of PPy/GO nanocomposites. Reproduced from Ref. [47] with permission from Elsevier.

Table 1.1 XRD results of graphite, GNS, and PE/graphite nanocomposites.

Sample	2θ (°)	d_{002} (nm)	Crystal size, C (nm)
Graphite flake	26.67	0.333	58.38
GNS	26.52	0.336	28.15
PE/graphite 1.2%	26.53	0.336	24.77
PE/graphite 5.6%	26.42	0.338	14.58

Reproduced from [48] with permission from Wiley Interscience.

1 wt%, d-spacing decreased and this was attributed to the strong $\pi-\pi$ interactions between graphene sheets that did not permit polymer intercalation.

Clay nanocomposites prepared by *in situ* polymerization are reported using many polymers such as PAs [51], PP [52], polybenzoxazine (PBz) [53], and polysulfone (PSU) [54]. Puffr *et al*. [51] reported the synthesis of PA-6, PA-8, PA-12, and MPA12 (N-methyl-polyamide 12)/organo-MMT nanocomposites. The MMT was modified by cationic exchange in which 12-aminododecanoic acid (ADA) was used to intercalate the clay mineral. The intercalated MMT with lactam monomers and ADA were blended together as a solid mixture, melted, and then sent to the glass ampoules for polymerization to take place at 260 °C. XRD results showed that the nanocomposites produced were exfoliated or with d-spacing higher than 6 nm. Regarding PP/clay nanocomposites,

Table 1.2 XRD results of graphene and PBT/graphene nanocomposites.

Sample	2θ (°)	d_{002} (Å)
Graphene	26.403	3.373
PBT/graphene 0.5%	26.348	3.380
PBT/graphene 0.75%	26.326	3.383
PBT/graphene 1%	26.408	3.372

Reproduced from [50] with permission from Elsevier.

different clay-supported magnesium/titanium ZN catalysts were used and were investigated by Dias *et al*. [52]. Slurry polymerizations at 70 °C and 2 bars were conducted to synthesize the nanocomposites. It was determined that the performance of the catalyst to yield exfoliated/intercalated structures depends on the clay mineral and the synthesis conditions. PBz/organo-modified MMT nanocomposites were synthesized by thermal ring-opening polymerization [53]. The intercalated benzoxazine (Bz)-MMT clay was first prepared by ion-exchange reaction and was then dispersed in fluid Bz monomers by mechanical stirring, as shown in Figure 1.19. The cast films were cured at 240 °C for 3 h in air oven for polymerization to take place. XRD and TEM results revealed that partially exfoliated/intercalated structures were obtained. Similarly, Dizman *et al*. [54] reported the synthesis of exfoliated/intercalated PSU/organo-modified MMT nanocomposites. They were achieved via *in situ* photo-induced cross-linking polymerization. Sixteen Philips 8W/06 lamps emitting light at $\lambda > 350$ nm were used as a source of irradiation. Figure 1.20 shows the TEM images of PSU/MMT nanocomposites in which "e" refers to exfoliation and "i" to intercalation.

Another composite synthesized via *in situ* polymerization is poly(ethylene terephthalate) (PET)/LDH by Cui *et al*. [55]. Terephthalate-intercalated LDH were first dispersed in ethylene glycol and then mixed with dimethyl terephthalate (DMT) and manganese acetate and magnesium acetate as catalysts. The synthesis was carried out in two steps: ester interchange reaction at 190–230 °C and polycondensation reaction at 280 °C. Partially exfoliated structures were achieved as revealed by morphological studies.

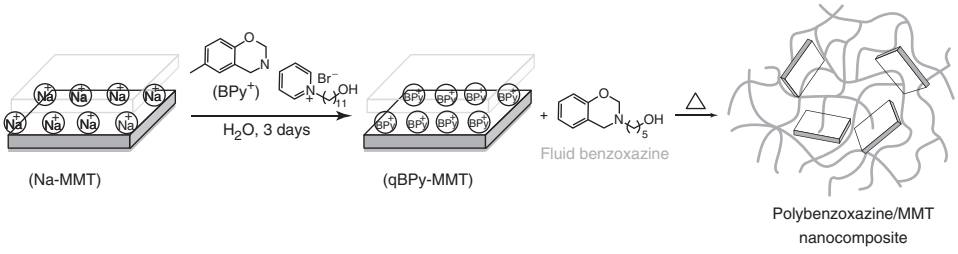

Figure 1.19 Schematic of PBz/MMT nanocomposite synthesis. Reproduced from [53] with permission from Wiley Periodicals.

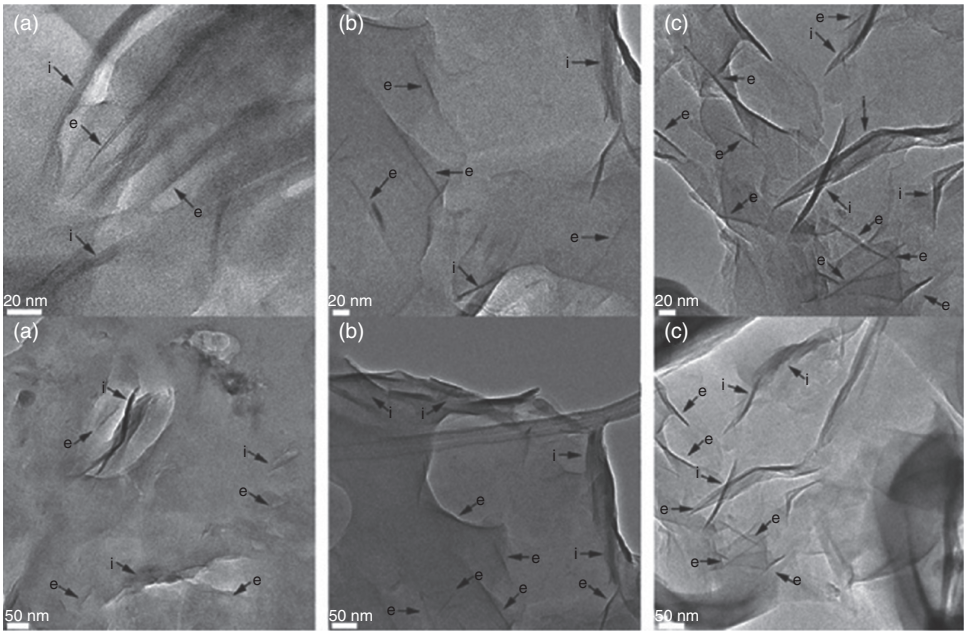

Figure 1.20 TEM images of PSU/MMT nanocomposites at: (a) 1 wt% (b) 3 wt% (c) 5 wt% in high magnification at top and low magnification at below images. Reproduced from [54] with permission from WILEY-VCH Verlag GmbH & Co. KGaA.

Dash *et al.* [56] reported the synthesis of poly(anthranilic acid) (PAnA)/MWCNT composites via *in situ* chemical oxidative polymerization. The CNTs were first functionalized using H_2SO_4 and HNO_3 to provide carboxylic acid groups at the surface. Then, the functionalized MWCNTs were sonicated in a 1.2-M HCl solution for 2 h before adding aniline and anthranilic acid to the suspension. Ammonium persulfate reagent in HCl solution was added to the mixture and mechanically stirred. The copolymer products obtained were filtered, washed, and vacuum dried. SEM analysis showed that the diameter of the nanocomposite increased with increasing MWNT loading as PAA coated itself on the outer surface of the nanotubes. This coating happened because of the strong interactions between the comonomer (i.e., aniline) and the functionalized MWNTs, as suggested by the authors. Using a similar procedure, Li and Kim [57] reported the synthesis of PANI/MWCNT composites for sensor applications. Core and shell structures were visible in SEM images, which signal the typical structure of polymer-grafted nanocomposites.

Wu and Liu [58] prepared PS/MWCNTs via solution-free radical *in situ* polymerization. Without any pretreatment of MWCNTs, they were combined with styrene monomers, toluene, and AIBN initiators. The mixture was heated at 90 °C for 11 h and the product was precipitated and vacuum dried. Fourier transform infrared (FTIR) spectroscopy analysis concluded the successful grafting of PS onto the walls of CNTs. Qualitative relationships between initiator and temperature

Table 1.3 Effect of polymerizing conditions on monomer conversion and polymer grafting percentages for PS nanocomposites.

MWCNTs-PS	Polymerizing temperature (°C)	AIBN added (g)	*C*% of St	PG%
1	90	0.01	9.9	2.9
2	90	0.02	30.5	4.9
3	90	0.05	39.0	15.6
4	90	0.10	55.2	4.2
5	90	0.15	58.3	0.8
6	90	0.20	59.7	0.8
7	80	0.5	34.1	2.2
8	70	0.5	19.0	1.5
9	60	0.5	13.1	0.9
10	50	0.5	9.0	0.6

Reproduced from [58] with permission from Taylor & Francis.

with monomer conversion and polymer grafting were established by the authors, as shown in Table 1.3.

1.2.4 Nontraditional Methods

In order to facilitate better dispersion of the filler in the polymer matrix for improved properties of final composites, researchers investigated different routes based on the traditional methods mentioned earlier. For instance, *in situ* polymerization can be customized to be redox [59, 60] or catalytic chain transfer [61] or even photo-induced polymerizations [54]. Others include microwave-induced synthesis [62, 63], one-pot synthesis [64–66], template-directed synthesis [67], electrochemical synthesis [68], self-assembly synthesis [69, 70], and intermatrix synthesis (IMS) [71–74].

As the name implies, one-pot synthesis refers to a sequence of reactions being carried out in the same reactor. As it refers to a location, this mode can be inclusive of other synthesis methods. For instance, Hwang *et al*. [66] reported the synthesis of tin (Sn)-embedded carbon-silica polymer nanocomposites. Even though it is a one-pot synthesis, the preparation was conducted via self-assembly method. Through the selective interaction of resol (carbon precursor), tetraethylorthosilicate (TEOS), and tributylphenyltin (Sn precursor) with an amphiphilic diblock copolymer, poly(ethylene oxide-b-styrene) (PEO-bPS), unique structures of nanowires, or nanoparticles, were achieved, as shown in Figure 1.21. It was reported that Sn was uniformly embedded in the rigid carbon-silica matrix.

Self-assembly, as the name implies, dictates the spontaneous arrangement of the existing components following local interactions among the components. As a result, ordered structures can be obtained as illustrated by Liu

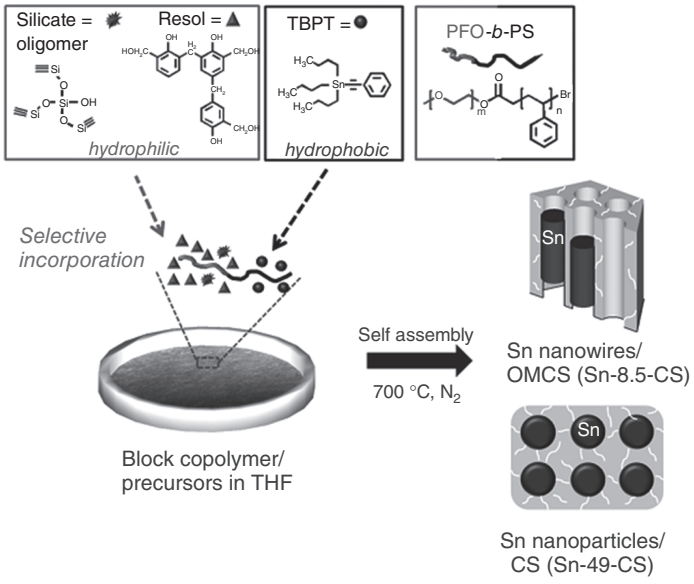

Figure 1.21 Schematic of Sn/carbon-silica composite synthesis. Reproduced from [66] with permission from American Chemical Society.

et al. [69]. Graphene-polymer composites were prepared by π−π stacking as shown in Figure 1.22. Pyrene-terminated Poly(2-N,N′-(dimethyl amino ethyl acrylate)) (PDMAEA) and pyrene-terminated poly(acrylic acid) (PAA) were first dissolved in aqueous graphene solution and sonicated. Excess polymer was removed by centrifugation at 14 000 rpm for 30 min. The precipitate was collected and redispersed in water to obtain the final composites. Layer-by-layer graphene-polymer composites were prepared by electrostatic interactions via self-assembly.

IMS is used to synthesize polymer stabilized metal nanoparticles (PSMNPs) [74]. In order to use this method, the polymer matrix must possess some functional groups capable of binding the nanoparticles. There are two versions in which IMS can be performed to prepare PSMNP-based sensors: in situ and ex situ [72]. The former deals with depositing the neat polymer onto the electrode surface followed by metal loading and metal reduction either by chemical or electrochemical means. The latter deals with dissolving the PSMNP-polymer nanocomposite in a solvent to form an ink. This ink can then be easily deposited on the electrode surface. Ruiz *et al*. [72] reported the synthesis of monometallic Pd-PSMNPs in sulfonated poly(ether ether ketone) (SPEEK) using intermatrix approach. It was noted that the properties of membranes prepared depended on the preparation route and reduction method. Conversely, Domènech *et al*. [74] stated that SPEEK possesses high hydrophilicity which limits its applications. Therefore, sulfonated polyethersulfone with Cardo group (SPES-C) was used as a polymer matrix to prepare catalytic membrane reactors by phase-inversion.

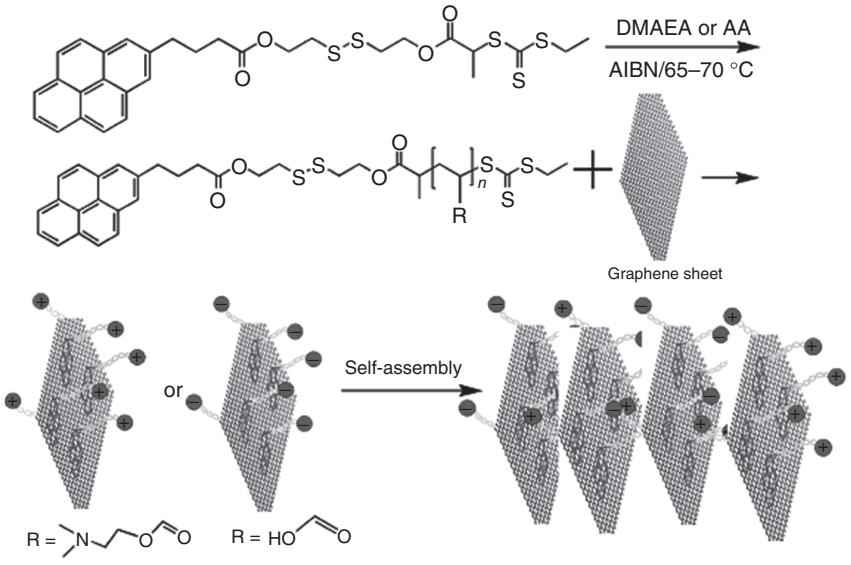

Figure 1.22 Schematic of graphene-polymer composite synthesis. Reproduced from [69] with permission from American Chemical Society.

In situ electrochemical synthesis is considered useful for the quick detection of current–voltage characteristics. Ameen *et al*. [68] reported the synthesis of PANI/graphene nanocomposites via this method. This synthesis was performed in a three-electrode system: fluorinated tin oxide glass (FTO) as working electrode, platinum wire as counter electrode, and reference electrode. Graphene oxide and aniline monomers were dispersed in HCl. This permitted the aniline to form its salt with a positive charge and to be adsorbed on to the surface of graphene oxide. Following the electrostatic interactions between the components, a homogeneous mixture of graphene oxide/aniline was obtained. The suspension was spread on FTO substrates by spin coat and then dried in a vacuum oven. The applied potential of −1.0 to +1.0 V with scan rate of 0.02 V s^{-1} was used for the oxidation and polymerization of aniline on the surface of graphene oxide and the simultaneous reduction to graphene. Figure 1.23 shows the Field-Emission scanning electron microscope (FESEM) and TEM images of graphene and the composite.

Microwave-assisted method has considerable advantages such as rapid volumetric heating, high reaction time, enhanced reaction selectivity, and energy saving behavior [62]. Cellulose–silver nanocomposites were prepared using microcrystalline cellulose and silver nitrate in ethylene glycol as a solvent [62]. In addition, ethylene glycol is useful as a reducing agent and a microwave absorber. Through this route, silver nanoparticles were formed in situ on the cellulose surface. According to SEM, silver particles were homogeneously dispersed in the cellulose substrate.

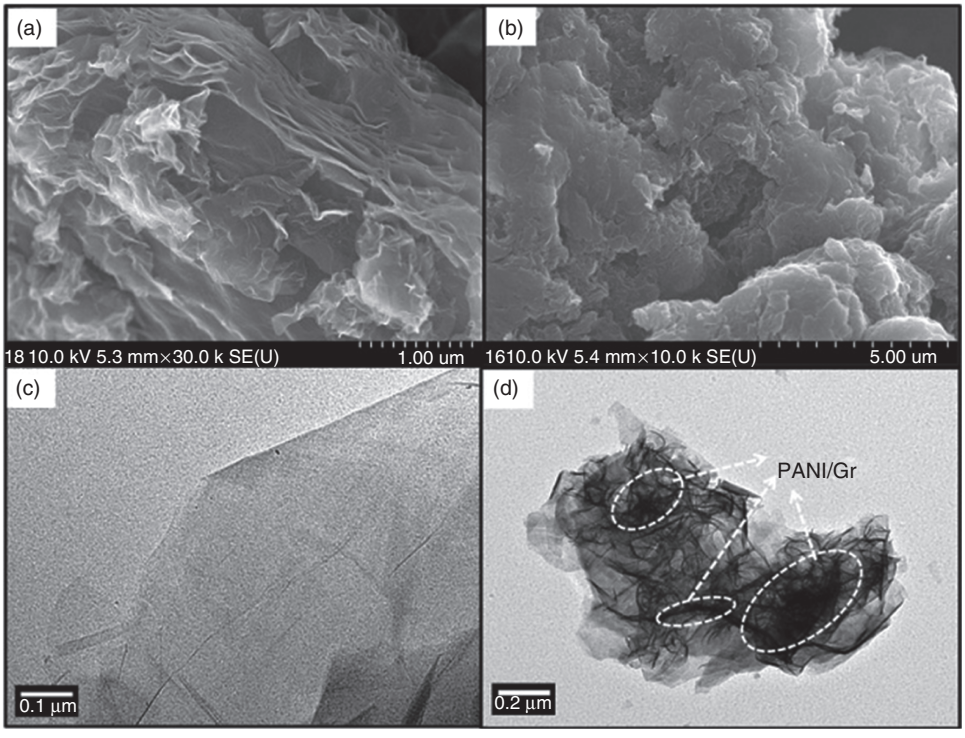

Figure 1.23 FESEM images of: (a) graphene, (b) PANI/graphene composite and TEM images of, (c) graphene, and (d) PANI/graphene composite. Reproduced from [68] with permission from Elsevier.

References

1. Mittal, V. (2010) in *Optimization of Polymer Nanocomposite Properties* (ed. V. Mittal), Wiley-VCH Verlag GmbH & Co. KGaA, Weinheim, pp. 1–19.
2. Ray, S.S. and Okamoto, M. (2003) Polymer/layered silicate nanocomposites: a review from preparation to processing. *Prog. Polym. Sci.*, **25**, 1539–1641.
3. Pavlidou, S. and Papaspyrides, C.D. (2008) A review on polymer-layered silicate nanocomposites. *Prog. Polym. Sci.*, **33**, 1119–1198.
4. Abedi, S. and Abdouss, M. (2014) A review of clay-supported Ziegler-Natta catalysts for production of polyolefin/clay nanocomposites through in situ polymerization. *Appl. Catal. Gen.*, **475**, 386–409.
5. Mittal, V. (2009) Polymer layered silicate nanocomposites: a review. *Materials*, **2**, 992–1057.
6. Alexandre, M. and Dubois, P. (2000) Polymer-layered silicate nanocomposites: preparation, properties and uses of a new class of materials. *Mater. Sci. Eng.*, **28**, 1–63.
7. Potts, J.R., Dreyer, D.R., Bielawski, C.W., and Ruoff, R.S. (2011) Graphene-based polymer nanocomposites. *Polymer*, **52**, 5–25.
8. Sahoo, N.G., Rana, S., Cho, J.W., Li, L., and Chan, S.H. (2010) Polymer nanocomposites based on functionalized

carbon nanotubes. *Prog. Polym. Sci.*, **35**, 837–867.

9. Spitalsky, Z., Tasis, D., Papagelis, K., and Galiotis, C. (2010) Carbon nanotube-polymer composites: chemistry, processing, mechanical and electrical properties. *Prog. Polym. Sci.*, **35**, 357–401.
10. Alig, I., Pötschke, P., Lellinger, D., Skipa, T., Pegel, S., Kasaliwal, G.R., and Villmow, T. (2012) Establishment, morphology and properties of carbon nanotube networks in polymer melts. *Polymer*, **53**, 4–28.
11. Junior, J.P.C., Soares, I.L., Luetkmeyer, L., and Tavares, M.I.B. (2014) Preparation of high-impact polystyrene nanocomposites with organoclay by melt intercalation and characterization by low-field nuclear magnetic resonance. *Chem. Eng. Process.: Process Intensifi.*, **77**, 66–76.
12. Labidi, S., Azema, N., Perrin, D., and Lopez-Cuesta, J.-M. (2010) Organo-modified montmorillonite/poly(ε-caprolactone) nanocomposites prepared by melt intercalation in a twin-screw extruder. *Polym. Degrad. Stab.*, **95**, 382–388.
13. Maiti, S., Suin, S., Shrivastava, N.K., and Khatua, B.B. (2014) Low Percolation threshold and high electrical conductivity in melt-blended polycarbonate/multiwall carbon nanotube nanocomposites in the presence of poly(ε-caprolactone). *Polym. Eng. Sci.*, **54**, 646–659.
14. Annala, M., Lahelin, M., and Seppälä, J. (2012) Utilization of poly(methyl methacrylate) – carbon nanotube and polystyrene – carbon nanotube *in situ* polymerized composites as masterbatches for melt mixing. *eXPRESS Polym. Lett.*, **6** (10), 814–825.
15. Wang, Z., Yang, X., Wei, J., Xu, M., Tong, L., Zhao, R., and Liu, X. (2012) Morphological, electrical, thermal and mechanical properties of phthalocyanine/multi-wall carbon nanotubes nanocomposites prepared by masterbatch dilution. *J. Polym. Res.*, **19** (9), 9969–9976.
16. Tan, J., Wang, X., Luo, Y., and Jia, D. (2012) Rubber/clay nanocomposites by combined latex compounding and melt mixing: a masterbatch process. *Mater. Des.*, **34**, 825–831.
17. Kutlu, B., Meinl, J., Leuteritz, A., Brünig, H., and Heinrich, G. (2013) Melt-spinning of LDH/HDPE nanocomposites. *Polymer*, **54**, 5712–5718.
18. Mezghani, K., Farooqui, M., Furquan, S., and Atieh, M. (2011) Influence of carbon canotube (CNT) on the mechanical properties of LLDPE/CNT nanocomposite fibers. *Mater. Lett.*, **65**, 3633–3635.
19. Shanks, R.A. and Cerezo, F.T. (2012) Preparation and properties of poly(propylene-g-maleic anhydride) filled with expanded graphite oxide. *Composites Part A*, **43**, 1092–1100.
20. Unnikrishnan, L., Mohanty, S., Nayak, S.K., and Ali, A. (2011) Preparation and characterization of poly(Methyl Methacrylate)–clay nanocomposites via melt intercalation: effect of organoclay on thermal, mechanical and flammability properties. *Mater. Sci. Eng. A*, **528**, 3943–3951.
21. Barick, A.K. and Tripathy, D.K. (2010) Thermal and dynamic mechanical characterization of thermoplastic polyurethane/organoclay nanocomposites prepared by melt compounding. *Mater. Sci. Eng. A*, **527**, 812–823.
22. Erceg, M., Jozic, D., Banovac, I., Perinovic, S., and Bernstorff, S. (2014) Preparation and characterization of melt intercalated poly(ethylene oxide)/lithium montmorillonite nanocomposites. *Thermochim. Acta*, **579**, 86–92.
23. Shen, Z., Simon, G.P., and Cheng, Y.-B. (2002) Comparison of solution intercalation and melt intercalation of polymer-clay nanocomposites. *Polymer*, **43**, 4251–4260.
24. Shawky, H.A., Chae, S.-R., Lin, S., and Wiesner, M.R. (2011) Synthesis and characterization of a carbon nanotube/polymer nanocomposite membrane for water treatment. *Desalination*, **272**, 46–50.
25. Araby, S., Meng, Q., Zhang, L., Kang, H., Majewski, P., Tang, Y., and Ma, J. (2014) Electrically and thermally conductive elastomer/graphene nanocomposites by solution mixing. *Polymer*, **55**, 201–210.

26. Bian, J., Wei, X.W., Lin, H.L., Gong, S.J., Zhang, H., and Guan, Z.P. (2011) Preparation and characterization of modified graphite oxide/poly(propylene carbonate) composites by solution intercalation. *Polym. Degrad. Stab.*, **96**, 1833–1840.
27. Paul, P.K., Hussain, S.A., Bhattacharjee, D., and Pal, M. (2013) Preparation of polystyrene-clay nanocomposite by solution intercalation technique. *Bull. Mater. Sci.*, **36** (3), 361–366.
28. Gu, Z., Song, G., Liu, W., Wang, B., and Li, J. (2009) Preparation and properties of organo-montmorillonite/cis-1,4-polybutadiene rubber nanocomposites by solution intercalation. *Appl. Clay Sci.*, **45**, 50–53.
29. Mahmood, N., Islam, M., Hameed, A., and Saeed, S. (2013) Polyamide 6/multiwalled carbon nanotubes nanocomposites with modified morphology and thermal properties. *Polymers*, **5**, 1380–1391.
30. Marroquin, J.B., Rhee, K.Y., and Park, S.J. (2013) Chitosan nanocomposite films: enhanced electrical conductivity, thermal stability, and mechanical properties. *Carbohydr. Polym.*, **92**, 1783–1791.
31. Zeng, C., Hossieny, N., Zhang, C., and Wang, B. (2010) Synthesis and processing of PMMA carbon nanotube nanocomposite foams. *Polymer*, **51**, 655–664.
32. Chen, L., Ozisik, R., and Schadler, L.S. (2010) The influence of carbon nanotube aspect ratio on the foam morphology of MWNT/PMMA Nanocomposite Foams. *Polymer*, **51**, 2368–2375.
33. Shirazi, Y., Tofighy, M.A., and Mohammadi, T. (2011) Synthesis and characterization of carbon nanotubes/poly vinyl alcohol nanocomposite membranes for dehydration isopropanol. *J. Membr. Sci.*, **378**, 551–561.
34. Chen, J., Jia, C., and Wan, Z. (2014) The preparation and electrochemical properties of MnO_2/Poly(3,4-ethylenedioxythiophene)/multiwalled carbon nanotubes hybrid nanocomposite and its application in a novel flexible micro-supercapacitor. *Electrochim. Acta*, **121**, 49–56.
35. Zaragoza-Contreras, E.A., Hernández-Escobar, C.A., Navarrete-Fontes, A., and Flores-Gallardo, S.G. (2011) Synthesis of carbon black/polystyrene conductive nanocomposite. pickering emulsion effect characterized by TEM. *Micron*, **42**, 263–270.
36. Hassan, M., Reddy, K.R., Haque, E., Minett, A.I., and Gomes, V.G. (2013) High-yield aqueous phase exfoliation of graphene for facile nanocomposite synthesis via emulsion polymerization. *J. Colloid Interface Sci.*, **410**, 43–51.
37. Hu, H., Wang, X., Wang, J., Wan, L., Liu, F., Zheng, H., Chen, R., and Xu, C. (2010) Preparation and properties of graphene nanosheets–polystyrene nanocomposites via in situ emulsion polymerization. *Chem. Phys. Lett.*, **484** (4–6), 247–253.
38. Kuila, T., Bose, S., Khanra, P., Kim, N.H., Rhee, K.Y., and Lee, J.H. (2011) Characterization and properties of in situ emulsion polymerized poly(methyl methacrylate)/graphene nanocomposites. *Compos. Part A: Appl. Sci. Manuf.*, **42** (11), 1856–1861.
39. Oh, M. and Kim, S. (2012) Effect of dodecyl benzene sulfonic acid on the preparation of polyaniline/activated carbon composites by in situ emulsion polymerization. *Electrochim. Acta*, **59**, 196–201.
40. Lin, Y., Ng, K.M., Chan, C.-M., Sun, G., and Wu, J. (2011) High-impact polystyrene/halloysite nanocomposites prepared by emulsion polymerization using sodium dodecyl sulfate as surfactant. *J. Colloid Interface Sci.*, **358** (2), 423–429.
41. Ye, Y., Chen, H., Wu, J., and Chan, C.M. (2011) Interlaminar properties of carbon fiber composites with halloysite nanotube-toughened epoxy matrix. *Compos. Sci. Technol.*, **71** (5), 717–723.
42. Cetintas, M. and Uyanık, N. (2013) Polystyrene-organoclay nanocomposites prepared via *in situ* emulsion polymerization. *Polym. Polym. Compos.*, **21** (3), 151–156.
43. Bhanvase, B.A., Pinjari, D.V., Gogate, P.R., Sonawane, S.H., and Pandit, A.B. (2012) Synthesis of exfoliated

poly(styrene-co-methyl methacrylate)/montmorillonite nanocomposite using ultrasound assisted in situ emulsion copolymerization. *Chem. Eng. J.*, **181–182**, 770–778.

44. Guo, Y., Bao, C., Song, L., Yuan, B., and Hu, Y. (2011) In situ polymerization of graphene, graphite oxide, and functionalized graphite oxide into epoxy resin and comparison study of on-the-flame behavior. *Ind. Eng. Chem. Res.*, **50**, 7772–7783.
45. Huang, Y., Qin, Y., Zhou, Y., Niu, H., Yu, Z.-Z., and Dong, J.-Y. (2010) Polypropylene/graphene oxide nanocomposites prepared by in situ ziegler-natta polymerization. *Chem. Mater.*, **22**, 4096–4102.
46. Potts, J.R., Lee, S.H., Alam, T.M., An, J., Stoller, M.D., Piner, R.D., and Ruoff, R.S. (2011) Thermomechanical properties of chemically modified graphene/poly(methyl methacrylate) composites made by in situ polymerization. *Carbon*, **49** (8), 2615–2623.
47. Bora, C. and Dolui, S.K. (2012) Fabrication of polypyrrole/graphene oxide nanocomposites by liquid/liquid interfacial polymerization and evaluation of their optical, electrical and electrochemical properties. *Polymer*, **53** (4), 923–932.
48. Fim, F.D.C., Guterres, J.M., Basso, N.R.S., and Galland, G.B. (2010) Polyethylene/graphite nanocomposites obtained by in situ polymerization. *J. Polym. Sci. Part A: Polym. Chem.*, **48** (3), 692–698.
49. Xu, Z. and Gao, C. (2010) In situ polymerization approach to graphene-reinforced nylon-6 composites. *Macromolecules*, **43** (16), 6716–6723.
50. Fabbri, P., Bassoli, E., Bon, S.B., and Valentini, L. (2012) Preparation and characterization of poly(butylene terephthalate)/graphene composites by in-situ polymerization of cyclic butylene terephthalate. *Polymer*, **53**, 897–902.
51. Puffr, R., Špátová, J.L., and Brožek, J. (2013) Clay mineral/polyamide nanocomposites obtained by in-situ polymerization or melt intercalation. *Appl. Clay Sci.*, **83–84**, 294–299.
52. Dias, M.L., Fernandes, R.M., Cunha, R.H., Jaconis, S., and Silvino, A.C. (2011) Highly filled clay polypropylene nanocomposites prepared by *in situ* polymerization with clay-supported magnesium/titanium catalysts. *Appl. Catal. Gen.*, **403** (1), 48–57.
53. Demir, K.D., Tasdelen, M.A., Uyar, T., Kawaguchi, A.W., Sudo, A., Endo, T., and Yagci, Y. (2011) Synthesis of polybenzoxazine/clay nanocomposites by *in situ* thermal ring-opening polymerization using intercalated monomer. *J. Polym. Sci. Part A: Polym. Chem.*, **49** (19), 4213–4220.
54. Dizman, C., Ates, S., Uyar, T., Tasdelen, M.A., Torun, L., and Yagci, Y. (2011) Polysulfone/clay nanocomposites by in situ photoinduced crosslinking polymerization. *Macromol. Mater. Eng.*, **296**, 1101–1106.
55. Cui, W., Jiao, Q., Zhao, Y., Li, H., Liu, H., and Zhou, M. (2012) Preparation of poly(ethylene terephthalate)/layered double hydroxide nanocomposites by *in situ* polymerization and their thermal property. *eXPRESS Polym. Lett.*, **6** (6), 485–493.
56. Dash, M.P., Tripathy, M., Sasmal, A., Mohanty, G.C., and Nayak, P. (2010) Poly(anthranilic acid)/multi-walled carbon nanotube composites: spectral, morphological, and electrical properties. *J. Mater. Sci.*, **45** (14), 3858–3865.
57. Li, W. and Kim, D. (2011) Polyaniline/multiwall carbon nanotube nanocomposite for detecting aromatic hydrocarbon vapors. *J. Mater. Sci.*, **46** (6), 1857–1861.
58. Wu, X. and Liu, P. (2010) Polymer grafted multiwalled carbon nanotubes via facile *in situ* solution radical polymerisation. *J. Exp. Nanosci.*, **5** (5), 383–389.
59. Chen, J., Qiao, J., Liu, H.-L., Yin, W.-Y., Fu, G.-C., and Zhang, Q.-F. (2011) A facile approach to polymer/clay nanocomposite by in situ redox polymerization. *Curr. Nanosci.*, **7** (4), 552–555.
60. Zhu, L., Liu, P., and Wang, A. (2014) High clay-content attapulgite/poly(acrylic acid) nanocomposite hydrogel via surface-initiated redox radical polymerization with modified attapulgite

nanorods as initiator and cross-linker. *Ind. Eng. Chem. Res.*, **53** (5), 2067–2071.

61. Chen, L., Wang, C., Li, Q., Yang, S., Hou, L., and Chen, S. (2009) In situ synthesis of transparent fluorescent ZnS–polymer nanocomposite hybrids through catalytic chain transfer polymerization technique. *J. Mater. Sci.*, **44** (13), 3413–3419.
62. Li, S.-M., Jia, N., Ma, M.-G., Zhang, Z., Liu, Q.-H., and Sun, R.-C. (2011) Cellulose–silver nanocomposites: microwave-assisted synthesis, characterization, their thermal stability, and antimicrobial property. *Carbohydr. Polym.*, **86** (2), 441–447.
63. Bogdal, D., Prociak, A., and Michalowski, S. (2011) Synthesis of polymer nanocomposites under microwave irradiation. *Curr. Org. Chem.*, **15** (2), 178–188.
64. Cao, J., Li, J., Liu, L., Xie, A.-J., Li, S., Qiu, L., Yuan, Y., and Shen, Y. (2014) One-pot synthesis of novel structure Fe_3O_4/Cu_2O/PANI nanocomposites as absorbents in water treatment. *J. Mater. Chem. A*, (**2**), 7953–7959.
65. Jo, C., Hwang, J., Song, H., Dao, A.H., Kim, Y.-T., Lee, S.H., Hong, S.W., Yoon, S., and Lee, J. (2013) Block-copolymer-assisted one-pot synthesis of ordered mesoporous WO_{3-x}/carbon nanocomposites as high-rate-performance electrodes for pseudocapacitors. *Adv. Funct. Mater.*, **23** (30), 3747–3754.
66. Hwang, J., Woo, S.H., Shim, J., Jo, C., Lee, K.T., and Lee, J. (2013) One-pot synthesis of tin-embedded carbon/silica nanocomposites for anode materials in lithium-ion batteries. *ACS Nano*, **7** (2), 1036–1044.
67. Müllner, M., Lunkenbein, T., Breu, J., Caruso, F., and Müller, A.H.E. (2012) Template-directed synthesis of silica nanowires and nanotubes from cylindrical core–shell polymer brushes. *Chem. Mater.*, **24** (10), 1802–1810.
68. Ameen, S., Akhtar, M.S., and Shin, H.S. (2012) Hydrazine chemical sensing by modified electrode based on *in situ* electrochemically synthesized polyaniline/graphene composite thin film. *Sens. Actuators, B*, **173**, 177–183.
69. Liu, J., Tao, L., Yang, W., Li, D., Boyer, C., Wuhrer, R., Braet, F., and Davis, T.P. (2010) Synthesis, characterization, and multilayer assembly of pH sensitive graphene–polymer nanocomposites. *Langmuir*, **26** (12), 10068–10075.
70. Wu, C., Huang, X., Wang, G., Lv, L., Chen, G., Li, G., and Jiang, P. (2013) Highly conductive nanocomposites with three-dimensional, compactly interconnected graphene networks via a self-assembly process. *Adv. Funct. Mater.*, **23** (4), 506–513.
71. Ruiz, P., Muñoz, M., Macanás, J., and Muraviev, D.N. (2010) Intermatrix synthesis of polymer–copper nanocomposites with tunable parameters by using copper comproportionation reaction. *Chem. Mater.*, **22** (24), 6616–6623.
72. Ruiz, P., Muñoz, M., Macanás, J., Turta, C., Prodius, D., and Muraviev, D.N. (2010) Intermatrix synthesis of polymer stabilized inorganic nanocatalyst with maximum accessibility for reactants. *Dalton Trans.*, **39** (7), 1751–1757.
73. Bastos-Arrieta, J., Muñoz, M., Ruiz, P., and Muraviev, D. (2013) Morphological changes of gel-type functional polymers after intermatrix synthesis of polymer stabilized silver nanoparticles. *Nanoscale Res. Lett.*, **8** (1), 1–4.
74. Domènech, B., Muñoz, M., Muraviev, D.N., and Macanás, J. (2011) Polymer-stabilized palladium nanoparticles for catalytic membranes: *ad hoc* polymer fabrication. *Nanoscale Res. Lett.*, **6** (1), 1–5.